



HAL
open science

Analysis of thermal dilution experiments with Distributed Temperature Sensing for fractured rock characterization

Maria Klepikova, Bernard Brixel, Delphine Roubinet

► **To cite this version:**

Maria Klepikova, Bernard Brixel, Delphine Roubinet. Analysis of thermal dilution experiments with Distributed Temperature Sensing for fractured rock characterization. *Journal of Hydrology*, 2022, 610, pp.127874. 10.1016/j.jhydrol.2022.127874 . insu-03658484

HAL Id: insu-03658484

<https://insu.hal.science/insu-03658484>

Submitted on 4 May 2022

HAL is a multi-disciplinary open access archive for the deposit and dissemination of scientific research documents, whether they are published or not. The documents may come from teaching and research institutions in France or abroad, or from public or private research centers.

L'archive ouverte pluridisciplinaire **HAL**, est destinée au dépôt et à la diffusion de documents scientifiques de niveau recherche, publiés ou non, émanant des établissements d'enseignement et de recherche français ou étrangers, des laboratoires publics ou privés.

Journal Pre-proofs

Research papers

Analysis of thermal dilution experiments with Distributed Temperature Sensing for fractured rock characterization

Maria Klepikova, Bernard Brixel, Delphine Roubinet

PII: S0022-1694(22)00449-8

DOI: <https://doi.org/10.1016/j.jhydrol.2022.127874>

Reference: HYDROL 127874

To appear in: *Journal of Hydrology*

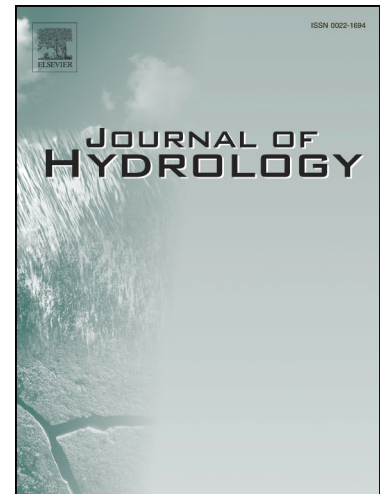
Received Date: 20 November 2021

Accepted Date: 21 April 2022

Please cite this article as: Klepikova, M., Brixel, B., Roubinet, D., Analysis of thermal dilution experiments with Distributed Temperature Sensing for fractured rock characterization, *Journal of Hydrology* (2022), doi: <https://doi.org/10.1016/j.jhydrol.2022.127874>

This is a PDF file of an article that has undergone enhancements after acceptance, such as the addition of a cover page and metadata, and formatting for readability, but it is not yet the definitive version of record. This version will undergo additional copyediting, typesetting and review before it is published in its final form, but we are providing this version to give early visibility of the article. Please note that, during the production process, errors may be discovered which could affect the content, and all legal disclaimers that apply to the journal pertain.

© 2022 Published by Elsevier B.V.



Analysis of thermal dilution experiments with Distributed Temperature Sensing for fractured rock characterization

Maria Klepikova^{a,*}, Bernard Brixel^b, Delphine Roubinet^c

^a*University of Rennes 1, CNRS, Géosciences Rennes, UMR 6118, Rennes, France*

^b*ETH Zurich, Geological Institute, Zurich, Switzerland*

^c*Géosciences Montpellier (UMR 5243), University of Montpellier, Montpellier, France*

Abstract

Thermal dilution experiments with Fiber-Optic Distributed Temperature Sensing (FO-DTS) were conducted at the In-situ Stimulation and Circulation (ISC) rock laboratory, at the Grimsel Test Site (GTS) in Switzerland. The experiment consists in replacing the total volume of a borehole with a warmer water and monitoring the rate of temperature increase and decrease during the heating and cooling periods, respectively. The changes in temperature monitored in depth and time under various hydraulic conditions and in different boreholes, are used to investigate the information provided by thermal dilution experiments in terms of groundwater flow and thermal properties in low-permeable fractured crystalline rock. The data analysis, and the use of analytical and numerical solutions for reproducing this data in the context of pure diffusion and advection-diffusion scenarios, lead to the following improvements and conclusions. (i) The formation thermal conductivity is estimated along the borehole by inverting the data collected under ambient conditions with a simple analytical solution. The estimated values are consistent with laboratory estimates. The method presents the advantage of requiring much shorter experiments than existing methods based on standard active-line-source (ALS) experiments, i.e., several hours versus the traditional 1-2 days. (ii) Hydraulically active fractures connecting boreholes

*Corresponding author

are detected from experiments conducted under cross-borehole forced hydraulic conditions. (iii) The formation thermal conductivity and fracture flow velocity have a distinguished impact on the temperature anomalies for some ranges of these property values, implying that both properties can be estimated from well-parametrized experiments.

Keywords: Fractured media, Fluid flow, Distributed temperature sensing, Thermal property estimates, Analytical and numerical solutions

1. Introduction

The use of fiber optic distributed temperature sensing (FO-DTS) in boreholes has seen a steep rise in popularity over the last fifteen years (Selker et al., 2006; Tyler et al., 2009). This is mainly motivated by efforts to integrate spatiotemporal measurements of subsurface temperatures in hydrogeological models (e.g., Anderson, 2005; Saar, 2010; Klepikova et al., 2014; Maldaner et al., 2019) and climate reconstruction studies (Freifeld et al., 2008). By now, commercial DTS systems can generate high-resolution temperature datasets with a measurement resolution of 0.01°C, reaching an effective spatial resolution along fibre optic cables up to 0.5 m when recording at a frequency of a few minutes (Simon et al., 2020).

Active-Distributed Temperature Sensing (A-DTS), which relies on the generation of a heat source in combination with distributed temperature measurements, is a promising method for characterizing the thermal properties of geologic material and monitoring subsurface fluid flow (e.g., Read et al., 2013; Liu et al., 2013; Bense et al., 2016; Maldaner et al., 2019; Simon et al., 2021). Changes in temperature detected at any given monitored location during heating or cooling periods are indicative of either the lithology or groundwater flow. In the absence of groundwater flow in or around the borehole, ~~A-DTS measurements~~ active thermal response tests, using classical temperature probes or DTS systems, can be used to estimate the formation's thermal conductivity (Pehme et al., 2007; Shehata et al., 2020). The pioneering work by Freifeld et al.

(2008), conducted in permafrost with no groundwater flow, demonstrated that A-DTS experiments can detect local variations in thermal conductivity with depth, yielding detailed thermal conductivity borehole-depth profiles. Built on this principle, thermal response tests using actively heated fiber optics have been considered as an advanced geothermal field investigation technique (Zhang et al., 2020).

Other field experiments also demonstrated that the rate of temperature increase and subsequent decrease during the heating and cooling periods of A-DTS experiments is sensitive to ambient groundwater flow (e.g., Sayde et al., 2015). Therefore, subsurface temperature responses also provide information about relative variations in horizontal groundwater flux rates (Liu et al., 2013; Klepikova et al., 2018). More recently, Simon et al. (2021) proposed interpretation methods of A-DTS experiments to quantify jointly porous media thermal conductivity values and groundwater fluxes in sediments.

The application of FO-DTS in fractured rock aquifers has been also explored in several studies. Hurtig et al. (1994) reported the first application of DTS to identify hydraulically-active fractures. Since then, several authors showed with different experimental configurations how A-DTS experiments can improve the identification of hydraulically active fractures together with the estimation of relative groundwater flow rates (Read et al., 2013; Pehme et al., 2013; Coleman et al., 2015). More recently, using a numerical model of groundwater flow and heat transport, Maldaner et al. (2019) presented a method to quantify the vertical distribution of local groundwater flow rates ~~in a borehole~~ through the bedrock fractures under natural gradient conditions. Based on this method, Munn et al. (2020) showed that changes in the magnitude of local fracture flow driven by cross-borehole pumping can also be quantified through A-DTS method. While these studies were able to estimate some ~~fluxes~~ through boreholes groundwater flow rates through hydraulically active fractures intersecting the borehole, the relatively coarse DTS spatial resolution, on order of 50 cm and more (Simon et al., 2020), still represents the limiting factor for such applications. The inadequacy of the spatial sampling with respect to the

desired objective (e.g., an accurate quantification of fluxes at the fracture scale)
55 implies that the original temperature signal is smoothed and information about
the depth-discrete fracture flow rate is often distorted.

Changes in temperature observed during A-DTS experiments also strongly
depend on how fibre-optics cables are deployed and how the thermal anomaly
is induced. This implies that in order to consider appropriate interpretation
60 methods, field experimental conditions should be carefully controlled (FO cable
position, heating duration, heating cable position if applicable), which can be
technically challenging. For example, most of the analytical solutions currently
used for the interpretation of A-DTS experiments assume that the heat source
is located at the borehole center, while the exact position of the heating and
65 fibre-optics cables, and the distance that separates them, are difficult to fix or
determine at depth (Lembcke et al., 2016). Yet such information is critical for
the estimation of the thermal properties. Theoretical estimations indicate that
even a small variation of the heat source position from its assumed position
can result in large errors in the relative thermal diffusivity estimate (Lembcke
70 et al., 2016). Another issue is that the application of the A-DTS method with
a line source of heat requires conducting long-term experiments. That includes
experiments using a heating element within the steel armoring of the fiber-optic
cable (Read et al., 2014; Bakx et al., 2019; Simon et al., 2020, 2021; Hakala
et al., 2022), a heating element separated from the fiber-optic cable (Freifeld
75 et al., 2008; Klepikova et al., 2018), or a composite cable design incorporating
parallel electrical conductors and optical fibers (Coleman et al., 2015). The
duration of the experiment in this case should be longer than the period of time
during which the temperature response is controlled by heat transfer occurring
through the borehole. For example, for a borehole in granite with a radius of 5
80 cm, the required duration of in-situ experiments for obtaining accurate estimates
of the thermal conductivity is in the order of 20 hours (Lembcke et al., 2016).
The two technical issues aforementioned can be solved by installing fiber-optic
and heating cables with direct push technology (Bakker et al., 2015; des Tombe
et al., 2019), but such installations are only possible in unconsolidated aquifers

85 (up to ~ 80 m).

As an alternative to a line source of heat, several studies proposed the physical injection of fluid with a contrasting temperature in order to introduce a thermal anomaly along the fibre length (Leaf et al., 2012; Read et al., 2013), also called thermal dilution tests. Injecting water with a contrasting temperature may be carried out to replace the total volume of a borehole (Read et al., 90 2013) or to create a discrete plume at a single borehole depth for a short period of time (Leaf et al., 2012). When the fluid inside a borehole is heated, assuming groundwater flow is negligible, the temperature decrease during the cooling period is only controlled by heat transfer occurring through the surrounding media, 95 which depends on the media's thermal properties. Nevertheless, the estimation of subsurface thermal properties from such measurements has typically relied upon numerical approaches valid only in specific applications. Consequently, this method suffers from the lack of a validated interpretation method, which is one of the objectives of the present study.

100 Finally, despite extensive success of A-DTS methods in high permeability settings (e.g., Leaf et al., 2012; Liu et al., 2013; Read et al., 2013; Pehme et al., 2013; Bakker et al., 2015; Maldaner et al., 2019; Simon et al., 2021), there has been no study to our knowledge reporting the application of A-DTS methods in low-permeability fractured media. Such investigations are critical to improve 105 our understanding of flow and heat transport processes in hydrogeological systems, Enhanced Geothermal Systems (EGS) and geologic nuclear waste repositories. To fill this gap, we performed a series of thermal dilution experiments in a well-characterized, sparsely fractured crystalline rock at the Grimsel Test Site (GTS) in Switzerland, where complementary data sets including core samples, 110 borehole geophysics, tracer and hydraulic tests exist for comparison and validation. We show here how space-time distributed temperature measurements with FO-DTS during thermal dilution experiments can be used to estimate thermal conductivity as a function of depth. To validate the approach, the thermal conductivity values derived from the A-DTS test are compared to the rock thermal 115 conductivity values measured in rock samples extracted from several boreholes

on site. We also propose a method to detect cross-flowing fractures between two boreholes and estimate in a qualitative manner the velocity of the fluid circulating in these fractures.

This paper is organized as follows. Section 2 describes the test facility, as well as the laboratory and field experiments. Section 3 describes the physical conceptualization and the implemented analytical and numerical approaches. The experimental, numerical and analytical results are presented and discussed in Section 4. Finally, Section 5 concludes with a summary of the most important findings.

2. Site and experimental description

2.1. Site Description

Thermal dilution experiments in this study were carried out as part of a unique series of hydraulic stimulations, known as the In-situ Stimulation and Circulation (ISC) experiment, aiming at a better understanding of hydro-seismo-mechanical coupled processes associated with a high-pressure fluid stimulation in granitic rock. The ISC experiment was conducted at the Grimsel Test Site (GTS), an underground rock laboratory constructed in the southern part of the Central Aar Massif, in the Swiss Alps (Figure 1a). The GTS is owned and operated by the Swiss National Cooperative for the Disposal of Radioactive Waste (NAGRA) and provides state-of-the-art facilities for in-situ experimentation in crystalline rock down to 0.5-km depth. The GTS is located in the crystalline rocks of the Central Aar Granite and Grimsel Granodiorite (Krietsch et al., 2018). The rocks of both lithologies are close to the mineralogical transition between granodioritic and granitic (Keusen et al., 1989; Kant et al., 2017; Krietsch et al., 2018). The matrix porosity is very low in crystalline rocks and ranges from 0.4 to 1 per cent (Krietsch et al., 2018). It is intersected by two major shear zone types: a set of reactivated ductile (S1) shear zones (depicted by orange surfaces in Figure 1) and a set of brittle-ductile (S3) shear zones (depicted by green surfaces in Figure 1). On a smaller scale, the support volume contains

145 a significant number of fractures with the degree of fracturing varying across
the site. The mean fracture density, measured from core and borehole logging,
was estimated to be low ($<1 \text{ m}^{-1}$) in the intact rock, and increasing up to 2.4
and 3 m^{-1} in the S1 and S3 shear zones, respectively (Brixel et al., 2020a). The
rock mass is accessed by 12 boreholes for measuring the seismic, hydraulic and
150 mechanical response to high-pressure fluid injections. For this study, measure-
ments only along two boreholes dedicated to high-pressure fluid injections (INJ1
and INJ2, shown by grey lines in Figure 1b) were conducted. The diameter of
boreholes is 0.146 m and the depth of the borehole is 44.7-44.8 m. The distance
between the two injection boreholes is 6 m and it increases with the distance
155 from the tunnel up to 12 m. A general overview of the experimental site as
well as the main concepts and the design of the ISC experiment can be found
in Amann et al. (2018). For more details on the hydrogeological and geological
conditions, see Jalali et al. (2018); Krietsch et al. (2018); Brixel et al. (2020a,b);
Klepikova et al. (2020).

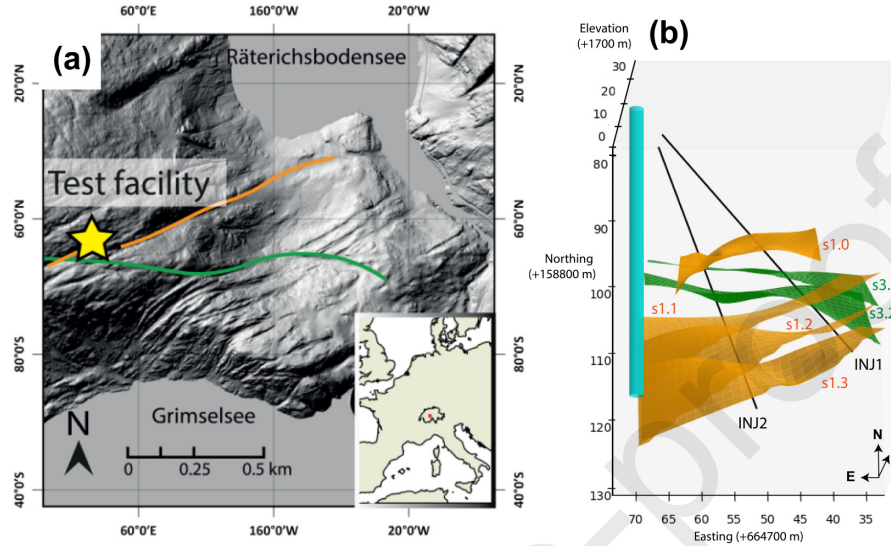


Figure 1: (a) Site location and main lineaments around the study area (modified from Brixel et al. (2020a)). (b) Geological model of the ISC experimental site (after Krietsch et al. (2018)) and configuration of injection boreholes, where the thermal dilution tests analyzed in the present study were completed. S1 and S3 fault zones are shown in orange and green, respectively.

160 2.2. Laboratory Rock Thermal Conductivity Measurements

The thermal conductivity measurements on rock core samples from the INJ1, INJ2 and PRP2 boreholes were performed at the hydrochemistry and contaminants laboratory of the Centre for Hydrogeology and Geothermics, Neuchatel, Switzerland. Note, that the PRP2 borehole (the diameter of boreholes is 0.131 m and the depth of the borehole is 45 m) was drilled in between INJ1 and INJ2 boreholes after the thermal dilution experiments were completed. We used the transient heat flow method (Von Herzen and Maxwell, 1959; Pribnow and Sass, 1995) performed by a TK04 Thermal Conductivity Meter (TeKa, Berlin, Germany, 2011). A modified line-source for plane surfaces is heated with constant power, and source temperature is recorded simultaneously. Thermal conductivity is calculated from the resulting heating curve (i.e., the rise of temperature

165
170

vs. time). The method yields absolute thermal conductivity values and does not require reference or calibration measurements. According to the manufacturer, the accuracy of the measuring device for thermal conductivity measurements is $\pm 3\%$. Out of 120 mm diameter rock cores, 9 samples were cut to an average thickness of 20 mm (the sample diameter should be at least equal to the probe diameter, 88 mm) for the analysis. After the preparation, the samples were air dried for several days. Considering very low porosity of rock samples, the difference in thermal conductivities for saturated and air dried samples should be negligible.

2.3. Thermal Dilution Test Design and Implementation

Thermal dilution tests were performed along the full length of both INJ1 and INJ2 boreholes. A similar method has been applied in a borehole section at the Ploemeur experimental site, in France (Read et al., 2013). To conduct the thermal dilution tests, a loop of BruSteel® cable (SOLIFOS Fiber Optic Systems, Switzerland), containing four multimode fibers encased in a sealed stainless steel capillary and covered by wire rope and a PVC jacket, was deployed for the continuous monitoring of temperature. A schematic showing the field deployment of the fiber optic equipment is presented in Figure 2a. Using cable ties (Figures 2c and d), the FO cable was mounted on a rigid PVC tube of 4 cm diameter, which could be screwed together in 2 m elements to the final length of 46 m. Once lowered, ~~the PVC tube was centralized at the top of the borehole, thus ensuring that the FO cable remained away from the borehole wall~~ this deployment insures a relatively constant off-center positioning of the FO cable inside the borehole. In order to maintain a proper bend radius of the fiber optic cable in the vicinity of the borehole bottom, we used a custom-built drop-shaped element shown in Figure 2b. The plastic tubing deployed in the monitoring borehole, was also used for the injection of the hot water. Tap water source from the facility main water line was heated using an electrical flow-through heater up to 45°C at surface and injected at the bottom of the borehole through the plastic tubing at a flow rate of about 10 L/min (resulting in a downhole injection temperature of

$\sim 36^\circ\text{C}$). Such injection temperature allows us to produce measurable changes in temperature while limiting buoyancy-driven borehole flow. To assure the replacement of the borehole volume with heated water, we injected ~ 1200 L of warm fluid, while the borehole volume ~ 750 L. During the injection, the water was naturally outflowing from ~~the borehole, while the hydraulic head in the borehole was monitored to verify that any changes were small enough to ensure no net flow in or out of~~ the borehole. After injection ceased, the temperature recovery was monitored for 4 hours under ambient hydraulic conditions and for 11 hours under cross-borehole flow hydraulic conditions.

A Silixa XT DTS unit was used for our dilution tests and configured to take single-ended temperature measurements with a spatial sampling interval of 0.25 m along the cable and an integration time of two minutes. The DTS temperature is calculated using the internal system calibration routine. To estimate the relative uncertainty of measurements, we used two external platinum reference thermometer sensors (PT100) with 0.1°C accuracy and one temperature transducer (RBR *solo* T) with 0.002°C accuracy co-located with a coiled 20 m section of fiber optic cable placed in an ice bath. The background groundwater temperature was recorded for at least 30 min before active borehole heating to establish a temperature baseline. The undisturbed vertical trend follows the natural geothermal gradient, $\sim 3^\circ\text{C}/100$ m (Figure .11). At the end of each thermal dilution test, pressure and temperature were allowed to recover prior to the start of the next experiment.

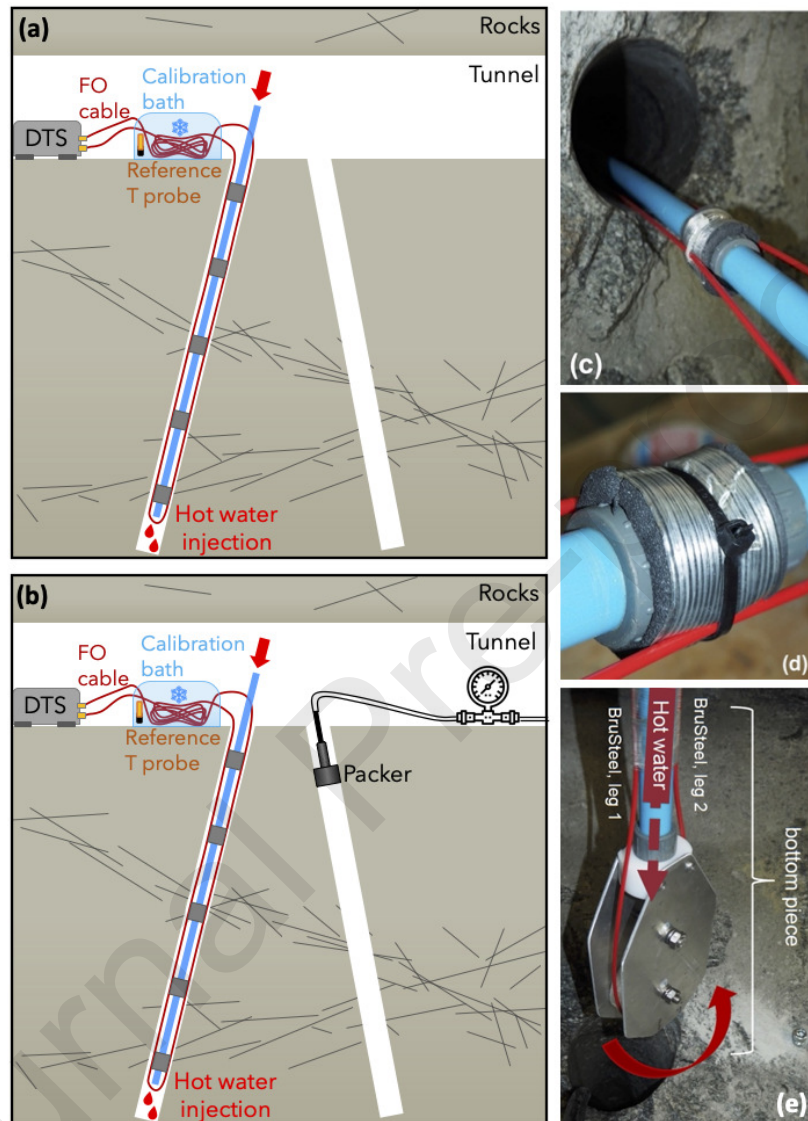


Figure 2: Schematic showing INJ1 and INJ2 boreholes in which the thermal dilution tests were conducted. The FO cable was mounted on a rigid plastic tubing and remained constant throughout each of the tests. Tests were carried out under both natural (a) and forced (i.e., cross-hole flow) conditions (b). For the case of forced hydraulic condition, an inflatable packer was placed at the top of the second borehole and tap water was injected through the packer under a constant pressure (b). Section of the A-DTS tool with the plastic tubing deployed in the monitoring borehole to maintain the FO cable close to the borehole center and for the injection of the hot water (c), the tube screw connections (d), and a custom-built drop-shaped element maintaining a proper bend radius of the fiber optic cable in the vicinity of the borehole bottom (e).

For experiments under forced hydraulic conditions, an inflatable packer was
225 placed at the top of the second borehole and tap water was injected through
the packer under a constant pressure (up to 4 bars for the INJ2 borehole and
up to 5.5 bars for the INJ1 borehole) immediately after the period of hot water
injection in the observation borehole. The temperature of the tap water was
almost identical to the average *in-situ* water temperature $\sim 12^\circ\text{C}$.

230 Following this procedure, three dilution tests were conducted in boreholes
INJ1 and INJ2 under various hydraulic conditions: (i) INJ2 was the tested
borehole (i.e., hot water is injected in borehole INJ2 and the depth temperature
profile was monitored in the same borehole during and after the injection) un-
der ambient hydraulic condition, (ii) INJ2 was again the tested borehole with
235 in this case forced hydraulic conditions that were applied by injecting water
in INJ1 after the heating period and (iii) INJ1 was the tested borehole with
forced hydraulic conditions that were applied by injecting water in INJ2 after
the heating period in INJ1. These experiments are denoted as *INJ2_ambient*,
INJ2_forced and *INJ1_forced*, respectively, in the rest of the manuscript.

240 3. Conceptual Model of Heat Transfer

The temperature anomaly created by the injection of a fluid with a contrast-
ing temperature propagates away from the borehole through a combination of
thermal conduction in intact rock mass (rock matrix), and advection driven by
groundwater flow at discrete location where hydraulically active fractures are
245 present (Figure 3). Furthermore, differences in hydraulic head between fracture
zones that connect to a borehole may create vertical borehole flow in between
fractures (Paillet, 1998; Klepikova et al., 2014). However, in the present study
we do not consider the effect of the vertical borehole flow on the thermal pattern,
as the effect of these bypass flows are minor compared to the horizontal heat
250 fluxes involved. To investigate which information can be extracted from the
A-DTS data, we consider in the following sections different conceptual models
of heat transfer that represent the two end-members of (i) pure diffusion (that

occurs away from an active fracture, Figure 3a-a'), and (ii) advection-diffusion (that occurs within an active fracture, Figure 3b-b').

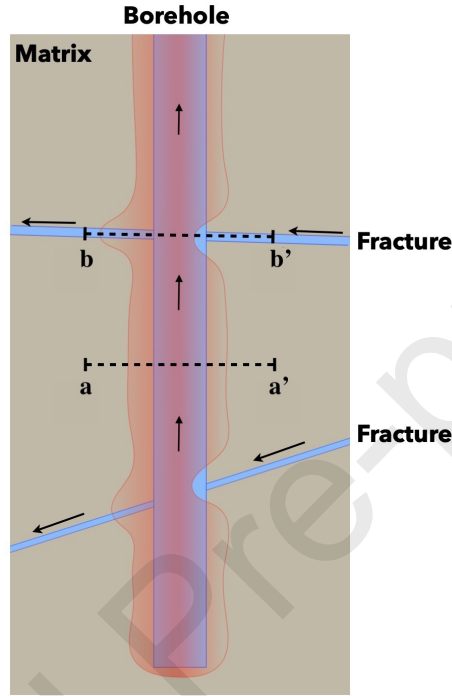


Figure 3: Schematic diagram showing the cooling phase during an A-DTS test. The fluid in the borehole is replaced with warmer water, creating a heat plume in water column in the borehole and the rock matrix. Hydraulically active fractures enhance heat dissipation. Note, that vertical bypass flows in the borehole between two active fractures can occur (depending of natural head difference between fractures).

255 3.1. Temperature Expressions for Pure Diffusion Scenario

Consider the borehole-matrix system presented in Figure 4 with the borehole and matrix domains defined in polar coordinates as $\Omega_b = \{(r, \theta) : 0 \leq r \leq R, 0^\circ \leq \theta \leq 360^\circ\}$ and $\Omega_m = \{(r, \theta) : R \leq r < \infty, 0^\circ \leq \theta \leq 360^\circ\}$, respectively. We assume pure thermal conduction in this system with initial thermal disequi-

260 librium between the borehole and matrix domains. K_i [W/(m°C)], ρ_i [kg/m³] and c_i [J/(kg°C)] denote the thermal conductivity, volumetric mass density and specific heat capacity, respectively, in the borehole ($i = 1$) and matrix ($i = 2$)

domains. Due to the system symmetry, the temperatures $T_1(r, t)$ and $T_2(r, t)$ in the borehole and matrix, respectively, do not depend on the angle variable θ .

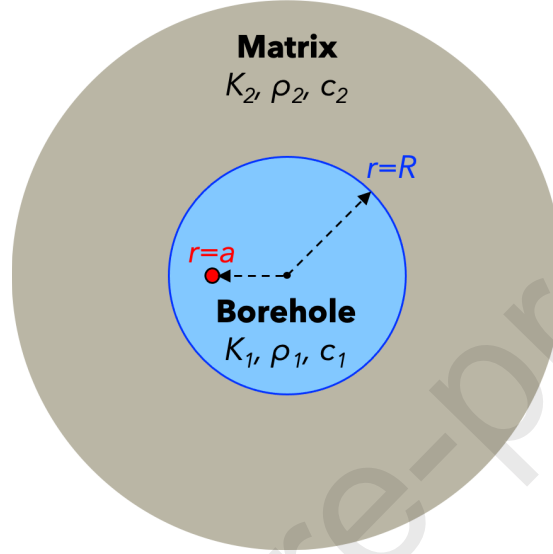


Figure 4: Cross section, from a top-down view, of a generic borehole-matrix system in polar coordinates with the temperature sensor (red circle) located at position $r = a$ inside the borehole of radius R . The borehole center is shown with a black dot.

265 Assuming that the system temperature is initially set to the constant temperature T_0 in the borehole and 0°C in the matrix, and that conduction is the only potential mechanism for horizontal heat transfer, applying temperature and heat-flux continuity conditions at the borehole-matrix interface ($r = R$) leads to the following temperature expressions in the Laplace domain (Carslaw
270 and Jaeger, 1986) (p.346, eq (4)-(5))

$$\bar{T}_1^*(r, p) = \frac{1}{p} - \frac{K_2 \sqrt{\kappa_1} \mathcal{K}_1(q_2 R) \mathcal{I}_0(q_1 r)}{p \Delta} \quad (1a)$$

$$\bar{T}_2^*(r, p) = \frac{K_1 \sqrt{\kappa_2} \mathcal{I}_1(q_1 R) \mathcal{K}_0(q_2 r)}{p \Delta} \quad (1b)$$

275 with $\bar{T}_1^*(r, p) = \bar{T}_1(r, p)/T_0$ and $\bar{T}_2^*(r, p) = \bar{T}_2(r, p)/T_0$, $\bar{T}_1(r, p)$ and $\bar{T}_2(r, p)$ being the Laplace transform of the temperatures $T_1(r, t)$ and $T_2(r, t)$ in the borehole and matrix, respectively, with the Laplace variable p . In expressions (1a)-

(1b), $\Delta = K_2\sqrt{\kappa_1}\mathcal{I}_0(q_1R)\mathcal{K}_1(q_2R) + K_1\sqrt{\kappa_2}\mathcal{I}_1(q_1R)\mathcal{K}_0(q_2R)$ with $\kappa_i = K_i/(\rho_i c_i)$
 280 and $q_i = \sqrt{p/\kappa_i}$ ($i = 1, 2$), and $\mathcal{I}_j(\cdot)$ and $\mathcal{K}_j(\cdot)$ are the modified Bessel functions
 of the first and second kind, respectively.

In the context of thermal dilution experiments, the temperature at the sensor
 position ($r = a$) can be evaluated by inverting expression (1a) into the standard
 time domain with numerical inversion methods such as the de Hoog's algorithm
 285 (de Hoog et al., 1982; Hollenbeck, 1998).

3.2. Numerical Modelling for Advection-Diffusion Scenario

To study the transfer of heat within active fractures (advection-diffusion sce-
 nario), we apply the finite element numerical modeling tool COMSOL Multiphysics
 (COMSOL Multiphysics User's Guide, Version 5.4., 2018) that simulates 2-D
 290 flow and heat transfer at the fracture-borehole intersection. The considered
 fracture-borehole system is presented in Figure 5. The 2-D domain has dimen-
 sions of 50 m \times 10 m with a 0.146 m diameter borehole located at the center
 of the domain. We assume constant laminar flow through the fracture along
 the x-axis. A no-flow boundary condition is applied to the two longitudinal
 295 boundaries along the flow direction. We assume that the fluid in the borehole is
 initially at temperature T_{ini} , while the temperature of the fluid in the fracture
 at $t = 0$ and at the outer boundaries at all times is T_{amb} . The domain was
 discretized into 430,000 elements and the element size varied from 0.002 m to
 0.1 m. The finer elements are located around the boreholes and the coarser
 300 elements are located near the boundaries of the rock matrix. Multiple model
 discretizations were performed to ensure mesh-independent results.

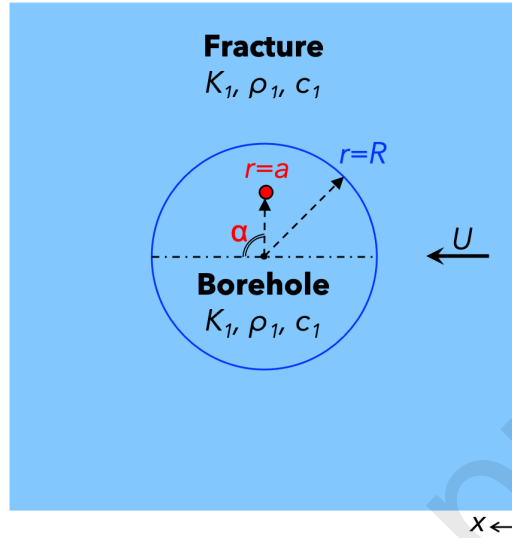


Figure 5: Cross section of a general borehole-fracture system with the temperature sensor (red circle) located at position $r = (a, \alpha)$ inside the borehole of radius R . The borehole center is shown with a black circle.

Considering advection-diffusion processes in the system, heat transport is described as follows:

$$\rho_1 c_1 \frac{\partial T}{\partial t} + \rho_1 c_1 \mathbf{U} \cdot \nabla T + \nabla \cdot \mathbf{q}^{(h)} = 0, \quad (2)$$

where the conductive heat flux is given by

$$\mathbf{q}^{(h)} = -K_1 \nabla T. \quad (3)$$

Here and in the following sections, \mathbf{U} denotes the local fluid velocity field [m/s]. Referred as the borehole properties in Section 3.1, K_1 , ρ_1 and c_1 denote the water thermal conductivity, density and specific heat capacity, respectively, and are defined as $K_1 = 0.59 \text{ W}/(\text{m}^\circ\text{C})$, $\rho_1 = 1000 \text{ kg}/\text{m}^3$ and $c_1 = 4189 \text{ J}/(\text{kg}^\circ\text{C})$.

4. Results and Discussion

310 4.1. Temperature response

The results from the thermal dilution experiments associated with ambient (*INJ2_ambient*) and forced flow (*INJ2_forced* and *INJ1_forced*) are shown in Figure 6. The middle panel in Figure 6 (second row) presents the absolute temperature values measured by FO-DTS, including the injection and cooling 315 phases. For all cases, $t = -2$ hours corresponds to the beginning of the hot water injection, which stops at $t = 0$ hours. By that time, the fluid in the borehole is replaced with water approximately 5 to 23°C warmer than the ambient temperature, which is approximately 12°C. By the end of the injection phase, temperature profiles exhibit a vertical gradient with no abrupt changes 320 in temperature gradient with higher post-injection temperatures at the bottom of the boreholes. Artifacts with warmer temperatures visible during the injection phase correspond to the leakage of injection warm water at the tube screw connections (Figure 2d). During the cooling phase, the thermal response is also variable with depth because of (i) the depth-variable initial conditions at $t = 0$ 325 and (ii) the depth variability of the rock thermal properties and/or magnitude of groundwater flow across the interval.

Similar to Read et al. (2013), we defined a Relative Temperature Anomaly (RTA) to account for the influence of the non-uniform borehole heating on the observed cooling rates as:

$$RTA(z, t) = \frac{T(z, t) - T_{amb}(z)}{T_{ini}(z) - T_{amb}(z)}, \quad (4)$$

where T_{amb} is the temperature prior to the start of the hot water injection and T_{ini} is the borehole temperature when the injection ceased. By doing so, we normalize the temperature anomaly between 0 and 1, where a value of 0 330 indicates a full recovery to the background groundwater temperature and a value of 1 corresponds to the initial temperature of the cooling period.

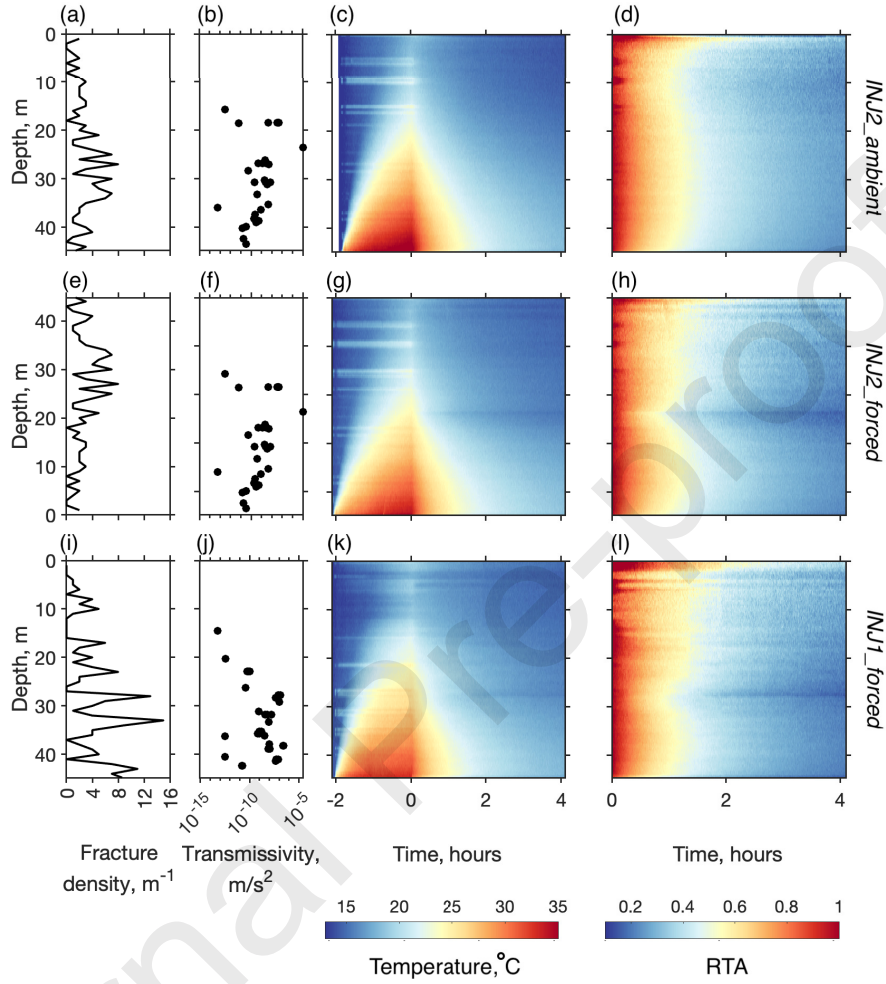


Figure 6: Fracture density (a,e,i) and transmissivity (b,f,j) depth profiles of the boreholes tested (Brixel et al., 2020a), (c,g,k) temperature depth profile along time in the tested borehole and (d,h,l) corresponding Relative Temperature Anomaly maps starting at $t = 0$ h. The first and second rows represent the experiments in which borehole INJ2 is tested under ambient (*INJ2_ambient*) and forced (*INJ2_forced*) conditions, respectively, and the third row the experiment in which INJ1 is tested under forced conditions (*INJ1_forced*).

For all tests, we observed that the cooling pattern is slightly different near the top of the borehole, which may be attributed to the contribution of variable-density driven free-convection in the borehole (Sammel, 1968; Klepikova et al.,

2018). Except this particular phenomenon, Figure 6c shows that under ambient
 conditions, the cooling in INJ2 borehole is relatively uniform. From Figures 6f
 and i it is evident that the injection in an adjacent well produces a detectable
 thermal effect, and heat dissipation is locally enhanced at 24 m in INJ2 borehole
 and 28 m in INJ1 borehole. As shown in Figures 6a, d and g, these zones coincide
 with transmissive fractures. For INJ1 borehole, the localized zone of enhanced
 cooling also coincides with a peak in fracture density, i.e., 15 fractures per meter
 (Figure 6i). The reported transmissivity values (Figure 6b,f,j) were obtained
 through high-resolution (i.e., intervals ≤ 1.0 m long) and discrete pressure pulse
 tests (≤ 2.5 m) (Brixel et al., 2020a). The fracture density (Figure 6a,e,i) was
 determined from borehole fracture traces identified from optical televiewer logs
 (Krietsch et al., 2018; Brixel et al., 2020a).

4.2. Thermal conductivity

In-situ estimates

In this section, we use temperature transients observed under the ambi-
 ent flow conditions to estimate rock thermal properties. We focus on the use
 of the analytical solution reported in Section 3.1 to reproduce the temperature
 evolution during the cooling phase of the experiment. Figure 7 shows the depth-
 average cooling transients measured during the experiment *INJ2_ambient* and
 converted to RTA according to Equation (4). The shaded area corresponds to
 one-sigma standard deviation between the temperature responses measured in
 depth at each time. It can be seen that the recorded rates of temperature do
 not vary significantly with depth. Using solution (1a), the thermal conductiv-
 ity was determined by minimizing the difference between analytically derived
 and observed water temperatures. Although the heat capacity and density of
 the rock matrix are both variable, such variations are typically smaller than
 variations in thermal conductivity, and constant values were chosen as reported
 by Kant et al. (2017), who performed the measurements in the vicinity of the
 Grimsel Test Site. The MATLAB function *fminsearch* was used to optimize
 the value of thermal conductivity that minimizes the root-mean-square error

365 (RMSE) between the average observed and analytically derived RTA. The fit that best describes our dataset (RMSE= 0.01°C) yields the thermal conductivity value of 2.65 W/m°C. The resulting curve fit is shown in Figure 7 as violet squares.

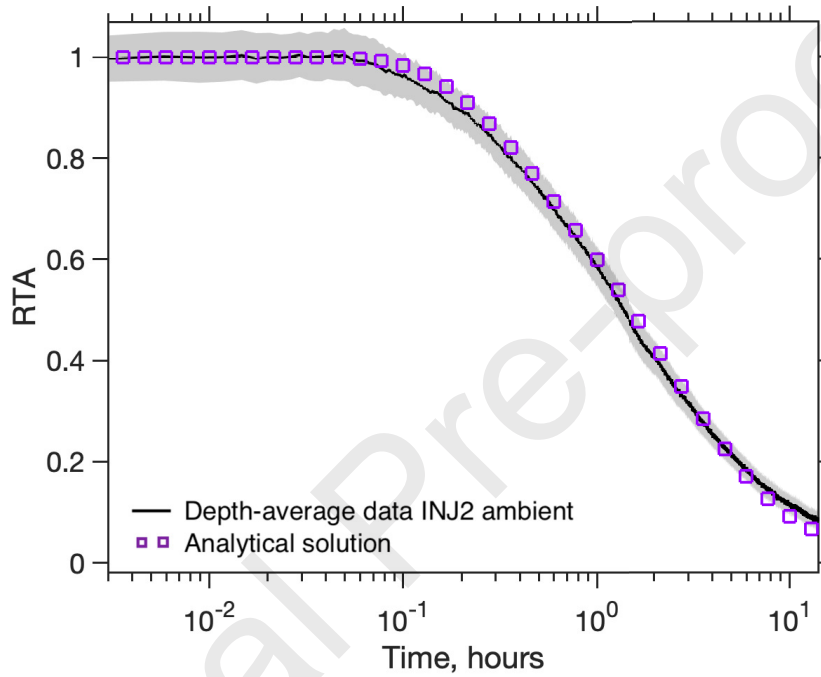


Figure 7: The depth-average Relative Temperature Anomaly measured in INJ2 (full borehole) under ambient conditions (black solid line) and one-sigma standard deviation between the temperature responses measured in depth at each time (shaded gray area). Magenta squares show data predicted using the developed analytical solution. Results for the best-fitting set of thermal properties are shown (RMSE= 0.01°C).

370 A deeper analysis of the data collected during experiment *INJ2_ambient* is done by inverting the thermal conductivity profile along depth from depth-discrete DTS temperature transients. The resultant profile is presented in Figure 8 showing the variability in depth of the estimated thermal conductivity. The high variability observed above 10 m with values ranging from 1.5 to 4 W/m°C, is related to the RTA anomalies observed at the top of the bore-

375 hole (Section 4.1). Overall, no significant variation with depth is observed, but
 the rock thermal conductivity does decrease slightly between the two S1 fault
 cores. An explanation for this slight decrease in the rock thermal conductivity
 could be an increased fracture density in the shear zones. Similar trend, i.e., a
 decrease of thermal conductivity with an increase of porosity induced by alter-
 380 ation and cracks, was already shown for the Soultz-sous-Forêts Granite (Surma
 and Géraud, 2003).

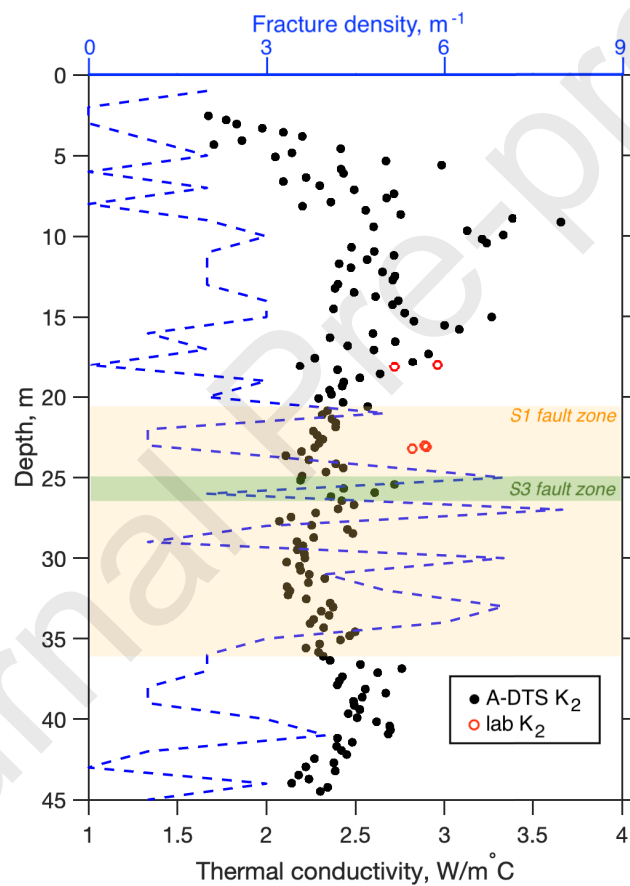


Figure 8: Thermal responses measured along 177 depth intervals (every 0.25 m) along the borehole INJ2 were used to invert the thermal conductivity profile. Lab-Measured rock thermal conductivity K_2 values (red circles) are provided for comparison. The blue dashed line indicates fracture density dept profile (relative to the upper axis). S1 and S3 fault zones are shown in orange and green, respectively.

Validation of the A-DTS-Derived Rock Thermal Properties

Laboratory measurements of drill core thermal conductivity are summarized in Table 1 and reported in Figure 8 for borehole INJ2. The results show rock thermal conductivity values varying from ~~2.542 to 2.964~~ 2.54 to 2.96 W/m°C, with average and median values of ~~2.806 and 2.825~~ 2.81 and 2.83 W/m°C, respectively. The measured values are in the range of already reported values for the Central Aar Granite and Grimsel Granodiorite (e.g., Keusen et al., 1989; Kant et al., 2017).

While the optimized thermal conductivity of the rock matrix is slightly lower than ranges measured in the laboratory ($K_2 = 2.65$ W/m°C), a close match between laboratory-derived and in-situ values is observed in Figure 8 for measurements collected in the rock formation. It demonstrates the efficacy of the proposed method to obtain reliable estimates of rock thermal conductivity from A-DTS experiments and shows that thermal dilution experiment allows us to determine rock thermal property estimates in situ.

Table 1: Lab-Measured rock thermal conductivity K_2 values of core samples from INJ1 INJ2 and PRP2 boreholes. Rows in grey correspond to the values from borehole INJ2 that are reported in Figure 8 with light and dark grey for samples that are located in the fault zone and formation, respectively.

| Sample ID | Borehole | Depth, m | K_2 , W/m°C |
|-----------|----------|----------|---------------|
| #1 | INJ2 | 23.0 | 2.90 |
| #2 | INJ2 | 23.1 | 2.90 |
| #3 | INJ2 | 23.2 | 2.83 |
| #4 | INJ1 | 35.0 | 2.54 |
| #5 | INJ1 | 35.1 | 2.84 |
| #6 | INJ1 | 35.2 | 2.78 |
| #7 | INJ2 | 18.0 | 2.96 |
| #8 | INJ2 | 18.1 | 2.72 |
| #9 | PRP2 | 2.6 | 2.77 |

4.3. RTA sensitivity to the presence of fluid flow

Figure 9 shows the depth-average Relative Temperature Anomaly (Equation (4)) measured under forced hydraulic conditions in INJ2 borehole (red dashed line), and INJ1 borehole (blue dashed line). For comparison, the black curve shows the depth-average RTA measured for all depths in INJ2 under ambient conditions. In all experiments, depth-average temperature transients follow a similar trend, suggesting homogeneous rock thermal properties and similar flow conditions. As expected, a notable exception is the data measured in INJ2 between 23 and 25 m bgs under forced hydraulic conditions. The corresponding temperature transient shown by red dashed line with stars in Figure 9 reveals a slightly enhanced rate of temperature decrease revealing the sensitivity of RTA to the presence of fluid flow in the fractured zone.

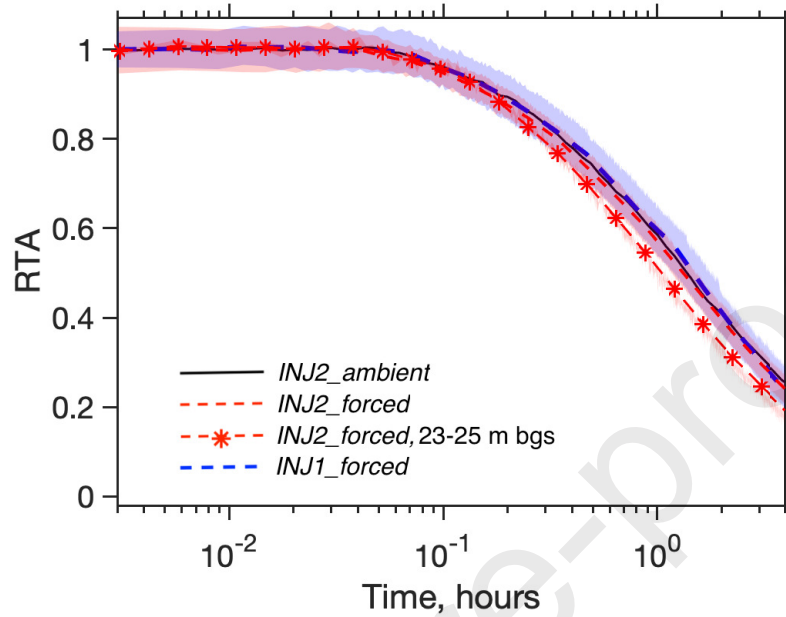


Figure 9: The depth-average Relative Temperature Anomaly measured in INJ2 while injecting in INJ1 for all depths (red dashed line) and for fracture zone depth (asterisks). Blue dashed line shows the depth-average Relative Temperature Anomaly measured in INJ1 while injecting in INJ2 for all depths. Shaded areas correspond to one-sigma standard deviation between all measured temperature responses at the specific time period. Black curve shows for comparison the depth-average Relative Temperature Anomaly measured for all depths in INJ2 under ambient conditions (Figure 7).

From these observations, we wish to evaluate which information, in terms of
 410 formation thermal conductivity and fracture flow velocity, we can extract from
 the data obtained in our A-DTS experiments. To investigate this, we consider
 two scenarios: pure diffusion scenario (Section 3.1) and advection-diffusion sce-
 nario (Section 3.2), and verify whether we can distinguish one scenario from the
 other with the A-DTS experiment data. In the first scenario, we consider realis-
 415 tic ranges of variation of the rock thermal conductivity $K_2 \in [K_2^{min}; K_2^{max}]$, and
 in the second scenario, realistic ranges of variation of the flow velocity in the
 fractures $U \in [U_{min}; U_{max}]$. For each scenario, the thermal response was calcu-
 lated by varying the corresponding parameter value over a large range while all

other parameters were fixed. The set of borehole and matrix properties, as well
 420 as the ranges of possible values used in the analytical and numerical solutions,
 are presented in Table 2.

Table 2: Water and matrix physical and thermal properties used in the analytical (pure diffusion, scenario 1) and numerical (advection-diffusion, scenario 2) solutions.

| Property/parameter | Values |
|--|--|
| Borehole radius R , m | 0.073 |
| FO cable location a , m | 0.05 |
| Water thermal conductivity K_1 , W/(m°C) | 0.59 |
| Water density ρ_1 , kg/m ³ | 1000 |
| Water specific heat capacity c_1 , J/(kg°C) | 4200 |
| Matrix density ρ_2 , kg/m ³ | 2550 |
| Matrix specific heat capacity c_2 , J/(kg°C) | 768 |
| Matrix thermal conductivity K_2 , W/(m°C), <i>scenario 1</i> | 2 to 5 |
| Flow velocity U , m/s, <i>scenario 2</i> | $1 \cdot 10^{-7}$ to $5 \cdot 10^{-4}$ |

Figure 10 shows the transient RTA calculated for the two scenarios and presented for different values of the parameters K_2 and U . As expected, the value of RTA depends on the media's thermal properties and groundwater flux.
 425 First, the groundwater flux has a strong impact on the thermal response (magenta domain in Figure 10). The tested range of groundwater flow (typically between 0.01 m/day to values greater than 10^2 m/day) corresponds to groundwater fluxes in sparsely fractured hard rocks (de Marsily, 1981). Beyond this range, the temperature increase is no more affected by flow variations. Moreover, the value of thermal conductivity strongly influences the value of RTA,
 430 since RTA varies by 10% over the tested range of thermal conductivity (blue domain in Figure 10).

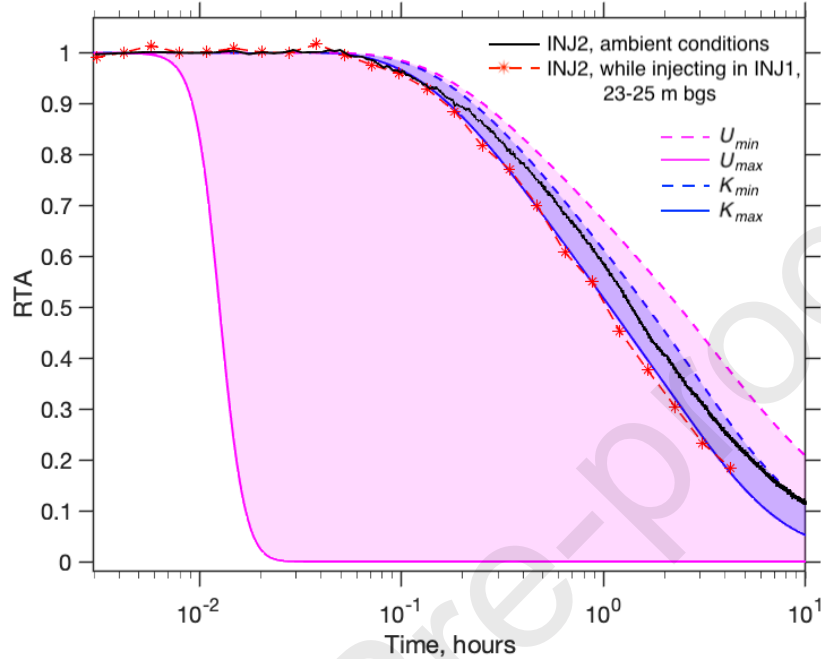


Figure 10: The transient RTA calculated analytically for the pure diffusion scenario with $K_2 \in [K_2^{min}; K_2^{max}]$ (blue domain) and numerically for the advection-diffusion scenario with $U \in [U_{min}; U_{max}]$ (magenta domain). The values of K_2 range from 2 W/m°C (blue dashed line) to 5 W/m°C (blue solid line) and the values of U range from $1 \cdot 10^{-7}$ (magenta dashed line) to $5 \cdot 10^{-4}$ (magenta solid line). For comparison, black curve shows the depth-average RTA measured for all depths in INJ2 under ambient conditions and red dashed-asterisks line shows the depth-average RTA measured in INJ2 while injecting in INJ1 for fracture zone depth.

The above results show that for some flow conditions, the resulting temperature transients obtained with the two scenarios overlap. This is the case when U varies from 1×10^{-6} m/s to 3×10^{-6} m/s, since the blue dashed and solid curves obtained for $K_2 = 2$ and 5 W/m°C, respectively, in the pure diffusion scenario, are also obtained for $U = 1 \times 10^{-6}$ m/s and 3×10^{-6} m/s in the advection-diffusion scenario. From this, we can consider that for small flow velocities ($U < 3 \times 10^{-6}$ m/s), the temperature response during A-DTS experiments does not allow to distinguish between pure diffusion scenario (Section

3.1) and advection-diffusion scenario (Section 3.2).

For comparison, Figure 10 also shows the depth-average RTA measured in INJ2 borehole under ambient flow conditions as well as the RTA observed under forced hydraulic conditions between 23 and 25 m bgs. Both curves fall within
 445 the overlapping domain, meaning that the observed faster cooling could be due to overlapping heat transfer processes. Thus, the faster cooling observed under forced hydraulic conditions in INJ2 between 23 and 25 m bgs and in INJ1 at 28 m bgs is potentially due to both advective flow in the fracture and/or due to the higher thermal diffusivity of the rock matrix at these depths. In
 450 order to plot a curve that overlap with the data, the thermal conductivity $K_{fr} = 5 \text{ W/m}^\circ\text{C}$ is required in the model with pure diffusion scenario, or the flow velocity $U_{fr} = 3 \cdot 10^{-6} \text{ m/s}$ is required in the model with advection-diffusion scenario. Nevertheless, as these zones of enhanced cooling can be readily distinguished only during cross-flow conditions, this effect would not be
 455 explained only by the contrast in thermal diffusivity, as the thermal diffusivity remains constant for the ambient and forced gradient tests. Consequently, the observed change in cooling can be attributed to a change in flow/velocity and is likely caused by groundwater flow through the fracture zones connected to the packed-off boreholes (Figure 2). Note, however, that given the relatively coarse
 460 spatial resolution of DTS units in comparison to fine-scale heterogeneities typical for fractured media, it is rarely possible to quantify the groundwater flow rate through individual fractures using A-DTS methods.

4.4. Sources of Uncertainty

In this section we discuss the major sources of uncertainties related to the
 465 developed method. Uncertainty on the thermal conductivity estimates may result from several unaccounted processes.

One of the potential sources of errors is related to non-isothermal conditions around the borehole by the end of the injection. When hot water is injected into the borehole, the heat plume propagates from the borehole into the matrix,
 470 with the intensity directly related to the injection duration and the downhole

temperature. Consequently, the rock matrix around the borehole bottom will be heated more rapidly than the shallow rock matrix. In order to minimize the influence of injection time on further estimation, ~~the duration of the injection should be shortened~~ more rapid injection to replace the borehole fluid should be favored. Furthermore, pumping from the top while injecting at the bottom may homogenize the water column temperature in the borehole.

Furthermore, temperatures in the borehole can be strongly influenced by the vertical borehole flow. This vertical flow results from advection due to differences in hydraulic head between large scale flow paths that are connected to the borehole ~~(?)~~ (Paillet, 1998) and/or from free convection caused by buoyancy force arising due to differences in fluid density (Sammel, 1968). First, due to a relatively low transmissivity of fractures, the effect of forced convection in the tested boreholes is expected to be minor compared to ~~diffusion and advection~~ conduction and advection of heat within the fractures. ~~This is further evidenced by~~ Furthermore, vertical flow within the borehole is assumed to be negligible because of the following observations: (1) ~~temperature measurements prior to the warm water injection presents a classical temperature evolution with depth according to the~~ under ambient conditions, the fluid temperature of the borehole follows that of the geothermal gradient (Figure .11); (2) ~~temperature transients observed during the A-DTS test~~ at the bottom ~~section~~ of the borehole ~~(no vertical flow expected)~~ follow a similar trend to those observed at the sections ~~between fractures (vertical flow may occur) suggesting similar flow below any transmissive fractures behave in a similar manner to the rest of the borehole where fractures exist suggesting minimal vertical flow along the borehole under ambient conditions;~~ (3) under forced conditions, where the nearby borehole is pumped, the temperature transient variability at the position of transmissive fractures is well above the variability measured in the ambient conditions.

Regarding the free-convection, in the beginning of the cooling period, the thermal gradients in the borehole are large enough to potentially result in free-convection in the borehole (e.g., $\sim 0.4^{\circ}\text{C}/\text{m}$). However, amplitudes of temperature oscillations at these gradients are no greater than $\sim 0.1^{\circ}\text{C}$ and their

magnitude is expected to decrease directly during later times, with the magnitudes of the thermal gradients (Sammel, 1968). The only exceptions are zones near the top of the boreholes with irregular cooling patterns and these zones were excluded from the fitting procedure.

5. Conclusions

In this paper, we propose thermal dilution experiment for characterizing fractured media heterogeneity. The method is based on the physical injection of fluid with a contrasting temperature in order to introduce thermal anomaly along the FO in open boreholes. First, we show that thermal dilution experiments are an effective approach to infer hydraulic connections between boreholes even in a low-permeability crystalline formation. Second, the method enables to obtain in-situ estimates of rock thermal conductivity with high spatial resolution. Compared to labor-intensive and time-consuming laboratory measurements or thermal conductivity, thermal dilution experiments are more suitable for effective thermal conductivity determination. Having in-situ estimates for the spatial distribution of thermal conductivity can improve our understanding of hydrogeological systems and reduce uncertainty in predictive modelling of EGS and geologic nuclear waste repositories. Importantly, the borehole thermal dilution experiments can be conducted for times much shorter than traditionally conducted active-line-source (ALS) experiments, as the temperature response during thermal dilution experiment is directly controlled by heat transfer occurring through the surrounding rock. Thus, the deployment process combined with the data collection may be completed within one day. In this paper, we apply analytical and numerical heat transfer models for interpreting borehole thermal experiments. Finally, our results demonstrate that for small flow velocities, the temperature response during A-DTS experiments does not allow to distinguish between a fracture flow setting and pure diffusion configuration, occurring away from an active fracture. This means that detection and quantification of groundwater flow from A-DTS experiment is only

possible for relatively high flow rates ($U > 3 \times 10^{-6}$ m/s). Overall, our results demonstrate that FO DTS allow a better understanding of both reservoir rock thermal properties and fluid flow in low permeability crystalline rocks.

Acknowledgements

535 The ISC is a project of the Deep Underground Laboratory at ETH Zurich, established by the Swiss Competence Center for Energy Research - Supply of Electricity (SCCER-SoE) with the support of the Swiss Commission for Technology and Innovation (CTI). Funding for the ISC project was provided by the ETH Foundation with grants from Shell and EWZ and by the Swiss Federal
540 Office of Energy through a P&D grant. The Grimsel Test Site is operated by Nagra, the National Cooperative for the Disposal of Radioactive Waste. We are indebted to Nagra for hosting the ISC experiment in their GTS facility and to the Nagra technical staff for onsite support. Maria Klepikova acknowledges financial support by ETH Zurich Career Seed Grant SEED-17. The authors
545 thank Martin Jung, Mohamadreza Jalali and René Dorrer for their help in the field. Maria Klepikova acknowledges Laurent Marguet and Benoît Valley for the access to Geothermics laboratory of the Centre for Hydrogeology and Geothermics (CHYN). The project has received funding from the European Union's Horizon 2020 research and innovation programme under the Marie-Sklodowska
550 Curie grant agreement No 838508.

References

- Amann, F., Gischig, V., Evans, K., Doetsch, J., Jalali, R., Valley, B., Krietsch, H., Dutler, N., Villiger, L., Brixel, B., Klepikova, M., Kittilä, A., Madonna, C., Wiemer, S., Saar, M.O., Loew, S., Driesner, T., Maurer, H., Giardini, D.,
 555 2018. The seismo-hydromechanical behavior during deep geothermal reservoir stimulations: open questions tackled in a decameter-scale in situ stimulation experiment. *Solid Earth* 9, 115–137. doi:10.5194/se-9-115-2018.
- Anderson, M.P., 2005. Heat as a ground water tracer. *Ground water* 43, 951–68. doi:10.1111/j.1745-6584.2005.00052.x.
- 560 Bakker, M., Caljé, R., Schaars, F., van der Made, K.J., de Haas, S., 2015. An active heat tracer experiment to determine groundwater velocities using fiber optic cables installed with direct push equipment. *Water Resources Research* 51, 2760–2772. doi:10.1002/2014WR016632.
- Bakx, Doornenbal, Weesep, Bense, Essink, Bierkens, 2019. Determining the
 565 relation between groundwater flow velocities and measured temperature differences using active heating-distributed temperature sensing. *Water* 11, 1619. doi:10.3390/w11081619.
- Bense, V.F., Read, T., Bour, O., Le Borgne, T., Coleman, T., Krause, S., Chalari, A., Mondanos, M., Ciocca, F., Selker, J.S., 2016. Distributed temperature sensing as a downhole tool in hydrogeology. *Water Resources Research*
 570 52, 9259–9273. doi:10.1002/2016WR018869.
- Brixel, B., Klepikova, M., Jalali, M.R., Lei, Q., Roques, C., Krietsch, H., Loew, S., 2020a. Tracking fluid flow in shallow crustal fault zones: 1. insights from single-hole permeability estimates. *Journal of Geophysical Research: Solid Earth* 125, e2019JB018200. doi:10.1029/2019JB018200.
 575
- Brixel, B., Klepikova, M., Lei, Q., Roques, C., Jalali, M.R., Krietsch, H., Loew, S., 2020b. Tracking fluid flow in shallow crustal fault zones: 2. insights from

- cross-hole forced flow experiments in damage zones. *Journal of Geophysical Research: Solid Earth* 125, e2019JB019108. doi:10.1029/2019JB019108.
- 580 Carslaw, H., Jaeger, J., 1986. *Conduction of Heat in Solids*. Oxford science publications, Clarendon Press.
- Coleman, T.I., Parker, B.L., Maldaner, C.H., Mondanos, M.J., 2015. Groundwater flow characterization in a fractured bedrock aquifer using active DTS tests in sealed boreholes. *Journal of Hydrology* 528, 449 – 462. doi:10.1016/j.jhydrol.2015.06.061.
- 585 COMSOL Multiphysics User's Guide, Version 5.4., 2018. COMSOL AB, Stockholm, Sweden. URL: <http://www.comsol.com>.
- Freifeld, B.M., Finsterle, S., Onstott, T.C., Toole, P., Pratt, L.M., 2008. Ground surface temperature reconstructions: Using in situ estimates for thermal conductivity acquired with a fiber-optic distributed thermal perturbation sensor. *Geophysical Research Letters* 35, 3–7. doi:10.1029/2008GL034762.
- 590 Hakala, P., Vallin, S., Arola, T., Martinkauppi, I., 2022. Novel use of the enhanced thermal response test in crystalline bedrock. *Renewable Energy* 182, 467–482. doi:10.1016/j.renene.2021.10.020.
- Hollenbeck, K.J., 1998. *Invlap.m*: A matlab function for numerical inversion of laplace transforms by the de Hoog algorithm.
- 595 de Hoog, F.R., Knight, J.H., Stokes, A.N., 1982. An improved method for numerical inversion of laplace transforms. *SIAM Journal on Scientific and Statistical Computing* 3, 357–366. doi:10.1137/0903022.
- 600 Hurtig, E., Grosswig, S., Jobmann, M., Kühn, K., Marschall, P., 1994. Fibre-optic temperature measurements in shallow boreholes: Experimental application for fluid logging. *Geothermics* 23, 355–364. doi:10.1016/0375-6505(94)90030-2.

- Jalali, M., Klepikova, M., Doetsch, J., Krietsch, H., Brixel, B., Dutler, N.,
605 Gischig, V., Amann, F., 2018. A Multi-Scale Approach to Identify and Characterize the Preferential Flow Paths of a Fractured Crystalline Rock. International Discrete Fracture Network Engineering Conference Day 3 Fri, June 22, 2018.
- Kant, M.A., Ammann, J., Rossi, E., Madonna, C., Höser, D., Rudolf von Rohr,
610 P., 2017. Thermal properties of Central Aare granite for temperatures up to 500°C: Irreversible changes due to thermal crack formation. Geophysical Research Letters 44, 771–776. doi:10.1002/2016GL070990.
- Keusen, H., Ganguin, J., Schuler, P., Buletta, M., 1989. Felslabor Grimsel Geologie Nagra Technischer Bericht NTB 87-14. 166. Technical Report. NAGRA
615 & GEOTEST.
- Klepikova, M., Brixel, B., Jalali, M., 2020. Transient hydraulic tomography approach to characterize main flowpaths and their connectivity in fractured media. Advances in Water Resources 136, 103500. doi:10.1016/j.advwatres.2019.103500.
- 620 Klepikova, M.V., Le Borgne, T., Bour, O., Gallagher, K., Hochreutener, R., Lavenant, N., 2014. Passive temperature tomography experiments to characterize transmissivity and connectivity of preferential flow paths in fractured media. Journal of Hydrology 512, 549–562. doi:10.1016/j.jhydro1.2014.03.018.
- 625 Klepikova, M.V., Roques, C., Loew, S., Selker, J., 2018. Improved characterization of groundwater flow in heterogeneous aquifers using granular polyacrylamide (pam) gel as temporary grout. Water Resources Research 54, 1410–1419. doi:10.1002/2017WR022259.
- Krietsch, H., Doetsch, J., Dutler, N., Jalali, M., Gischig, V., Loew, S., Amann,
630 F., 2018. Comprehensive geological dataset describing a crystalline rock mass for hydraulic stimulation experiments. Scientific Data 5, 180269. doi:10.1038/sdata.2018.269.

- Leaf, A.T., Hart, D.J., Bahr, J.M., 2012. Active Thermal Tracer Tests for Improved Hydrostratigraphic Characterization. *Ground Water* 50, 726–735. doi:10.1111/j.1745-6584.2012.00913.x. 635
- Lembcke, L., Roubinet, D., Gidel, F., Irving, J., Pehme, P., Parker, B., 2016. Analytical analysis of borehole experiments for the estimation of subsurface thermal properties. *Advances in Water Resources* 91, 88–103. doi:10.1016/j.advwatres.2016.02.011.
- 640 Liu, G., Knobbe, S., Butler Jr., J., 2013. Resolving centimeter-scale flows in aquifers and their hydrostratigraphic controls. *Geophysical Research Letters* 40, 1098–1103. doi:10.1002/grl.50282.
- Maldaner, C.H., Munn, J.D., Coleman, T.I., Molson, J.W., Parker, B.L., 2019. Groundwater flow quantification in fractured rock boreholes using active distributed temperature sensing under natural gradient conditions. *Water Resources Research* 55, 3285–3306. doi:10.1029/2018WR024319. 645
- de Marsily, 1981. *Hydrogéologie quantitative / par G. de Marsily,...* Collection Sciences de la terre, Masson, Paris.
- Munn, J.D., Maldaner, C.H., Coleman, T.I., Parker, B.L., 2020. Measuring 650 fracture flow changes in a bedrock aquifer due to open hole and pumped conditions using active distributed temperature sensing. *Water Resources Research* 56, e2020WR027229. doi:10.1029/2020WR027229.
- Paillet, F.L., 1998. Flow modeling and permeability estimation using borehole flow logs in heterogeneous fractured formations. *Water Resources Research* 34, 997–1010. doi:10.1029/98WR00268. 655
- Pehme, P., Greenhouse, J., Parker, B., 2007. The active line source temperature logging technique and its application in fractured rock hydrogeology. *Journal of Environmental & Engineering Geophysics* 12. doi:10.2113/JEEG12.4.307.
- Pehme, P., Parker, B., Cherry, J., Molson, J., Greenhouse, J., 2013. Enhanced 660 detection of hydraulically active fractures by temperature profiling in lined

heated bedrock boreholes. *Journal of Hydrology* 484, 1 – 15. doi:10.1016/j.jhydrol.2012.12.048.

Pribnow, D.F.C., Sass, J.H., 1995. Determination of thermal conductivity for deep boreholes. *Journal of Geophysical Research: Solid Earth* 100, 9981–9994. doi:10.1029/95JB00960.

665

Read, T., Bour, O., Bense, V., Le Borgne, T., Goderniaux, P., Klepikova, M., Hochreutener, R., Lavenant, N., Boschero, V., 2013. Characterizing groundwater flow and heat transport in fractured rock using fiber-optic distributed temperature sensing. *Geophysical Research Letters* 40, 2055–2059. doi:10.1002/grl.50397.

670

Read, T., Bour, O., Selker, J.S., Bense, V.F., Borgne, T.L., Hochreutener, R., Lavenant, N., 2014. Active-distributed temperature sensing to continuously quantify vertical flow in boreholes. *Water Resources Research* 50, 3706–3713. doi:10.1002/2014WR015273.

Saar, M.O., 2010. Review: Geothermal heat as a tracer of large-scale groundwater flow and as a means to determine permeability fields. *Hydrogeology Journal* 19, 31–52. doi:10.1007/s10040-010-0657-2.

675

Sammel, E.A., 1968. Convective flow and its effect on temperature logging in small-diameter wells. *GEOPHYSICS* 33, 1004–1012. doi:10.1190/1.1439977.

680

Sayde, C., Thomas, C.K., Wagner, J., Selker, J., 2015. High-resolution wind speed measurements using actively heated fiber optics. *Geophysical Research Letters* 42, 10064–10073. doi:10.1002/2015GL066729.

Selker, J.S., Thévenaz, L., Huwald, H., Mallet, A., Luxemburg, W., van de Giesen, N., Stejskal, M., Zeman, J., Westhoff, M., Parlange, M.B., 2006. Distributed fiber-optic temperature sensing for hydrologic systems. *Water Resources Research* 42. doi:10.1029/2006WR005326.

685

- 690 Shehata, M., Heitman, J., Ishak, J., Sayde, C., 2020. High-resolution measurement of soil thermal properties and moisture content using a novel heated fiber optics approach. *Water Resources Research* 56, e2019WR025204. doi:10.1029/2019WR025204.
- Simon, N., Bour, O., Lavenant, N., Porel, G., Nauleau, B., Pouladi, B., Longuevergne, L., 2020. A comparison of different methods to estimate the effective spatial resolution of FO-DTS measurements achieved during sandbox
695 experiments. *Sensors* 20, 570. doi:10.3390/s20020570.
- Simon, N., Bour, O., Lavenant, N., Porel, G., Nauleau, B., Pouladi, B., Longuevergne, L., Crave, A., 2021. Numerical and experimental validation of the applicability of active-dts experiments to estimate thermal conductivity and groundwater flux in porous media. *Water Resources Research* 57,
700 e2020WR028078. doi:10.1029/2020WR028078.
- Surma, F., Géraud, Y., 2003. Porosity and thermal conductivity of the soultz-sous-forêts granite. *pure and applied geophysics* 160, 1125–1136.
- TeKa, Berlin, Germany, 2011. TK04 Thermal Conductivity Meter User's Manual Version 5.0.
- 705 des Tombe, B.F., Bakker, M., Smits, F., Schaars, F., van der Made, K.J., 2019. Estimation of the variation in specific discharge over large depth using distributed temperature sensing (DTS) measurements of the heat pulse response. *Water Resources Research* 55, 811–826. doi:10.1029/2018WR024171.
- 710 Tyler, S.W., Selker, J.S., Hausner, M.B., Hatch, C.E., Torgersen, T., Thodal, C.E., Schladow, S.G., 2009. Environmental temperature sensing using raman spectra dts fiber-optic methods. *Water Resources Research* 45. doi:10.1029/2008WR007052.
- Von Herzen, R., Maxwell, A.E., 1959. The measurement of thermal conductivity of deep-sea sediments by a needle-probe method. *Journal of Geophysical
715 Research (1896-1977)* 64, 1557–1563. doi:10.1029/JZ064i010p01557.

Zhang, B., Gu, K., Shi, B., Liu, C., Bayer, P., Wei, G., Gong, X., Yang, L., 2020. Actively heated fiber optics based thermal response test: A field demonstration. *Renewable and Sustainable Energy Reviews* 134, 110336. doi:10.1016/j.rser.2020.110336.

720 Appendix

The background groundwater temperature was recorded for at least 30 min before the injection of hot water to establish a temperature baseline. The undisturbed vertical trend follows the natural geothermal gradient, $\sim 3^{\circ}\text{C}/100\text{ m}$. These temperature profiles follow the geothermal gradient, thus revealing that
 725 the effect of vertical borehole flows on the temperature distribution within observation boreholes is negligible.

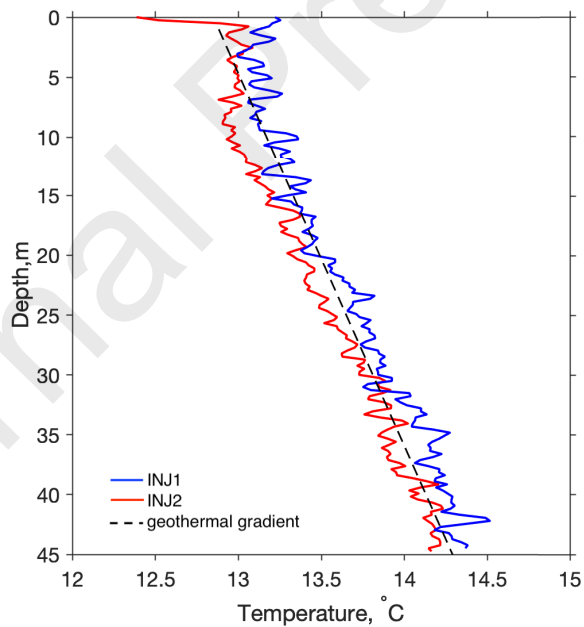


Figure .11: Borehole temperature profiles collected in INJ1 (blue line) and INJ2 (red line) boreholes before active borehole heating. The black dashed line represents the geothermal gradient.